Cell Reports
Physical Science

CellPress
OPEN ACCESS

Article

Energizing Fuel Cells with an Electrically Rechargeable Liquid Fuel

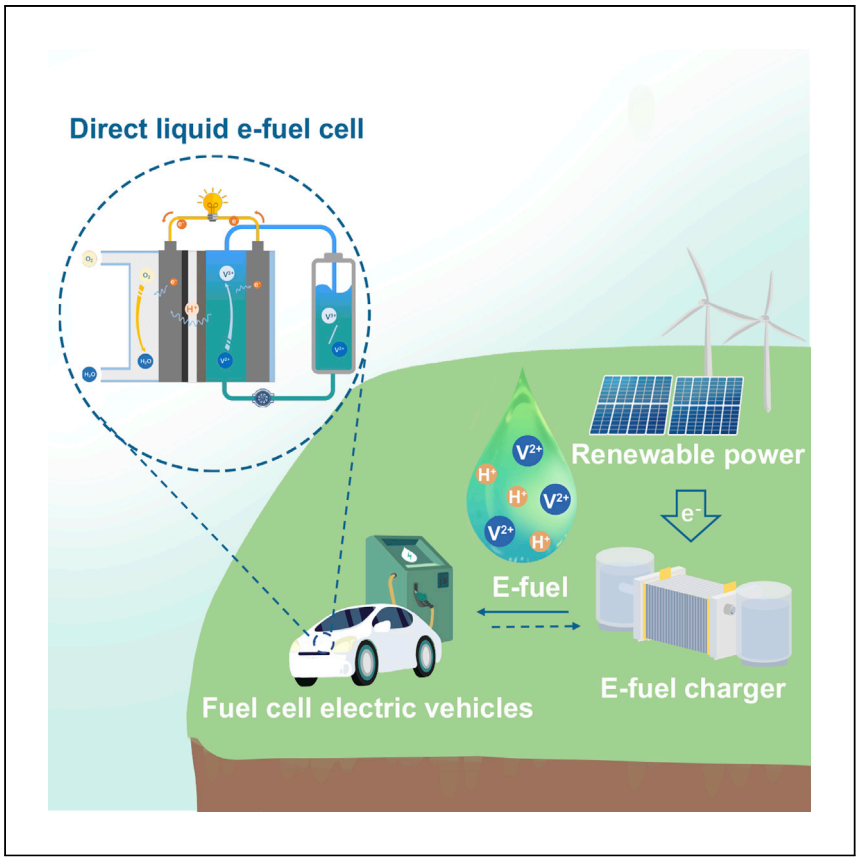

Shi et al. demonstrate an e-fuel cell capable of converting an electrically rechargeable liquid fuel into electricity. They achieve a peak power density of 293 mW cm^{-2} and an energy efficiency of 42.3% at room temperature, thus demonstrating the potential for powering future electric vehicles.

Xingyi Shi, Xiaoyu Huo, Yining Ma, Zhefei Pan, Liang An

liang.an@polyu.edu.hk

HIGHLIGHTS

An e-fuel cell fed with an electrically rechargeable liquid fuel is demonstrated

It consists of a catalyst-free graphite-felt anode and a conventional oxygen cathode

A peak power density of 293 mW cm^{-2} and an energy efficiency of 42.3% are achieved

Shi et al., Cell Reports Physical Science 1, 100102
July 22, 2020
https://doi.org/10.1016/j.xcrp.2020.100102

Cell Reports
Physical Science

CellPress
OPEN ACCESS

Article

Energizing Fuel Cells with an Electrically Rechargeable Liquid Fuel

Xingyi Shi,[1] Xiaoyu Huo,[1] Yining Ma,[1] Zhefei Pan,[1] and Liang An[1,2,*]

SUMMARY

Direct liquid fuel cells with high energy density and facile fuel storage have received increasing attention. Owing to the poor reactivity of conventional liquid fuels, they not only require noble metal catalysts for their oxidation but also exhibit limited performance. Here, we report a power-generation system, the direct liquid e-fuel cell, where "e-fuel" stands for "electrically rechargeable fuel." This e-fuel cell consists of a catalyst-free graphite-felt anode and a conventional oxygen cathode separated by a proton exchange membrane, producing a maximum current density of 750 mA cm^{-2}, a peak power density of 293 mW cm^{-2}, and an energy efficiency of 42.3% at room temperature, which is much higher than the performances achieved by conventional direct liquid fuel cells. This emerging technology, capable of fast recharging, could be a powerful, efficient, cost-effective, and durable power-generation device, showing great potential for commercialization in the fuel cell electric vehicle industry.

INTRODUCTION

In the last decade, the rising demand for the utilization of renewable energy has drawn more and more attention to energy conversion and storage systems. Among various energy conversion systems, the hydrogen fuel cell attributed to its high energy density and efficiency has been extensively studied[1–9] and applied in the electric vehicle industry for fuel cell electric vehicles (FCEVs). However, the widespread application of hydrogen fuel cells is restricted by many difficulties associated with the production, transportation, and storage of gaseous hydrogen.[10,11] As an alternative, therefore, direct liquid fuel cells (DLFCs) have received ever-increasing attention and become one of the most promising power sources for portable electric devices and FCEVs, primarily because unlike gaseous hydrogen, liquid fuels are energy dense and easy and safe to store and transport as gasoline.[10,12–15] However, most of these developed DLFCs must use noble metal catalysts for liquid fuel oxidation reactions but yield limited fuel cell performance, as shown in Tables S1[16–24] and S2,[16,20–23,25–31] greatly hindering their widespread application.[32–37]

Recently, the T.S. Zhao research group at The Hong Kong University of Science and Technology proposed an electrically rechargeable liquid fuel (e-fuel) concept, and it has attracted worldwide attention.[38,39] Radically different from conventional liquid fuels such as methanol and ethanol, this e-fuel is typically made of various electroactive species, including inorganic materials (e.g., metal ions), organic materials (e.g., alloxazines), and suspensions of particles (e.g., polysulfide-based nanofluid). Compared to conventional liquid fuels, this e-fuel offers three major advantages.[38] First, this e-fuel can be recharged and recycled by a simple electrochemical reaction, greatly reducing the e-fuel production cost of the e-fuel cell system. It was reported

[1]Department of Mechanical Engineering, The Hong Kong Polytechnic University, Hung Hom, Kowloon, Hong Kong SAR, China

[2]Lead Contact

*Correspondence: liang.an@polyu.edu.hk

https://doi.org/10.1016/j.xcrp.2020.100102

that the e-fuel solution can be used for >100 cycles, showing a coulombic efficiency of ~98% and a capacity decay rate of 0.1% per cycle, thus proving its excellent rechargeability.[38] Second, this e-fuel shows a high electrochemical reactivity even on carbon-based materials, thereby eliminating the use of any noble metal catalysts, which not only dramatically reduces the cell fabrication cost of the e-fuel cell but also greatly improves the e-fuel cell durability. Third, many liquid fuels (e.g., ethanol) suffer from the difficulty of breaking strong C–C bonds on the existing electrocatalysts, seriously limiting the fuel cell power density and energy efficiency, while this e-fuel exhibits faster kinetics and complete oxidation (typically, one-electron transfer process), dramatically boosting the e-fuel cell performance and in turn reducing the e-fuel cell system cost per unit power.

Although Li-ion battery technology has achieved great success during its commercialization process and has become the most widely used power source in battery electric vehicles (BEVs),[40–42] its low energy capacity and long recharging duration seriously restrict the travel distance of BEVs and their market penetration.[43–45] In comparison, the e-fuel cell system can independently alter its storage capacity (via changing the e-fuel volume and concentration) and power (via changing the electrode size), respectively. Meanwhile, the e-fuel cell system can be recharged by simply replacing the exhausted e-fuel solution with a fresh one, like refueling gasoline, which greatly shortens the recharging time.

Inspired by the e-fuel concept, here, we demonstrate a direct liquid e-fuel cell fed with the e-fuel solution as fuel and the pure oxygen as oxidant. Like conventional fuel cells, this e-fuel cell has a sandwich-like structure consisting of a catalyst-free graphite-felt anode and a conventional oxygen cathode separated by a proton exchange membrane. In addition, the e-fuel cell system includes an e-fuel-oxygen delivery system and other external accessories, as illustrated in Figure 1A. It has been demonstrated that the present e-fuel cell exhibits an open-circuit voltage (OCV) of 1.23 V, a maximum current density of 750 mA cm^{-2}, a peak power density of 293 mW cm^{-2}, and an energy efficiency of 42.3% at room temperature. Hence, the above-mentioned advantages make the present e-fuel cell system a promising candidate for powering FCEVs in the future.

RESULTS AND DISCUSSION

Working Principle

The e-fuel cell structure consists of a membrane electrode assembly (MEA) clamped by a pair of graphite plates containing a serpentine flow channel, as shown in Figure 1. The MEA consists of a catalyst-free graphite felt anode, a proton exchange membrane, and a conventional oxygen cathode. The e-fuel cell system contains an e-fuel cell, an e-fuel tank, an oxygen cylinder, and other accessories. During the e-fuel cell operation, the e-fuel solution containing V^{2+} ions is pumped into the anode flow channel, and then V^{2+} ions transport to the porous anode, where V^{2+} ions are oxidized to V^{3+} ions and electrons according to Equation 1:[46]

$$V^{2+} \rightarrow V^{3+} + e^{-} \qquad E_a^0 = -0.26V \qquad \text{(Equation 1)}$$

Then, electrons will travel through the external circuit and arrive at the cathode while protons in the anolyte will migrate through the membrane to the cathode to complete the circuit. On the cathode, oxygen is supplied to the cathode flow channel and then transported to the porous cathode, where the oxygen reduction reaction (ORR) takes place according to Equation 2:[46]

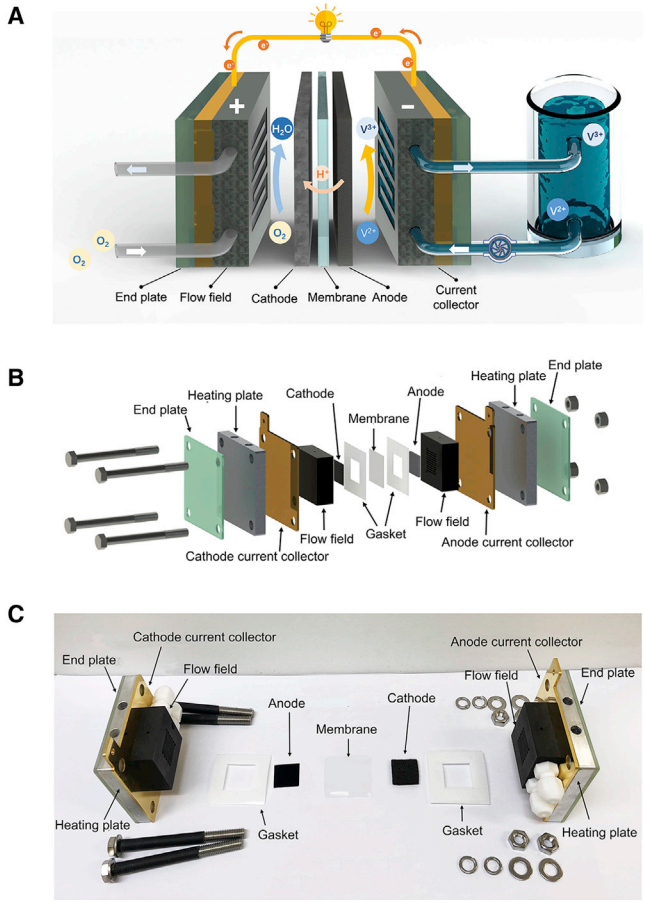

Figure 1. Scheme of an E-fuel Cell

(A) Working principle of an e-fuel cell.

(B and C) Design (B) and fabrication (C) of an e-fuel cell.

$$\frac{1}{4}O_2 + H^+ + e^- \rightarrow \frac{1}{2}H_2O \qquad E_c^0 = +\ 1.23V \qquad \text{(Equation 2)}$$

Hence, combining two reactions on the anode and cathode results in an overall reaction:[46]

$$V^{2+} + \frac{1}{4}O_2 + H^+ \rightarrow V^{3+} + \frac{1}{2}H_2O \qquad E^0 = 1.49V \qquad \text{(Equation 3)}$$

This e-fuel cell, fed with the electrolyte containing V^{2+} ions and pure oxygen, offers a theoretical voltage of as high as 1.49 V, which is much higher than those of many conventional DLFCs, such as direct ethanol fuel cells (1.14 V),[47,48] direct methanol fuel cells (1.21 V),[49,50] and direct ethylene glycol fuel cells (1.09 V),[51] creating an energy-dense electrochemical power-generation system.

Physical and Chemical Characterization of E-fuel Cell Electrodes

The surface morphologies of the catalyst-free graphite-felt anode and the conventional oxygen cathode were characterized by the scanning electron microscope (SEM). It is seen from Figures 2A and 2B that the catalyst-free graphite-felt anode was built with its interconnected carbon fibers,[52] thereby eliminating the use of noble metal catalysts.[53,54] Figures 2C and 2D show the surface morphology of the conventional oxygen cathode (Pt/C-coated carbon paper), in which a dense layer of

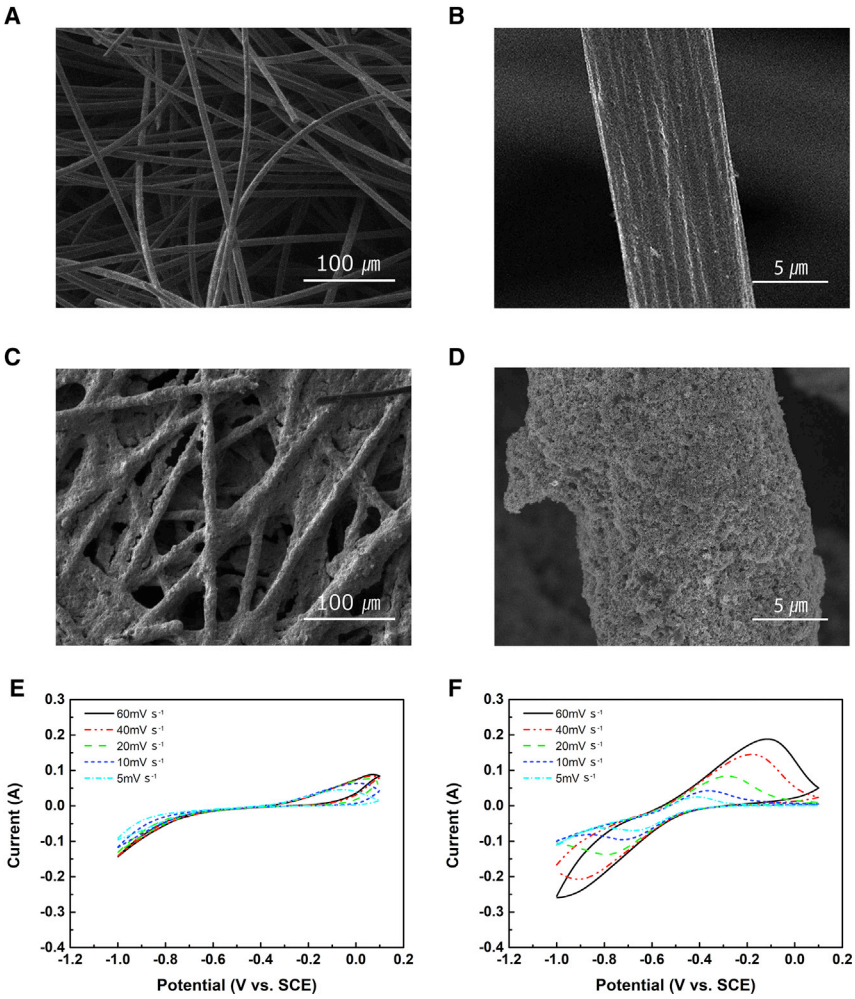

Figure 2. Physical and Chemical Characterization of 2 Electrodes

(A–D) Surface morphologies of the catalyst-free graphite-felt anode: (A) top surface view (scale bar, 100 μm), (B) single fiber level (scale bar, 5 μm), and the conventional oxygen cathode (C) top surface view (scale bar, 100 μm) and (D) single fiber level (scale bar, 5 μm).

(E and F) Electrochemical kinetics of the catalyst-free graphite-felt electrode (E) before and (F) after thermal treatment.

catalyst nanoparticles is coated on the whole surface of the carbon fibers and the porous structure and high specific area are believed to be retained. To evaluate the electrochemical performance improvement of the catalyst-free graphite-felt anode after thermal treatment, a cyclic voltammetry (CVs) test was carried out at different scan rates and the results are shown in Figures 2E and 2F. Without thermal treatment, there is no distinct oxidation peak corresponding to the oxidation of the V^{2+} ions. In contrast, a clear and high anodic peak appears after thermal treatment, indicating that the e-fuel solution is highly reactive on the thermally treated graphite-felt electrode even without using any noble metal catalysts. Such an improvement in performance after the thermal treatment is mainly attributed to the following aspects: (1) the reaction between oxygen and graphite felt creates oxygen functional groups (e.g., hydroxyl functional groups), which can accelerate the vanadium-ion oxidation;[55] (2) meanwhile, the reaction will also create numerous pores on the surface and thus enlarge the specific surface area;[56] and (3) the

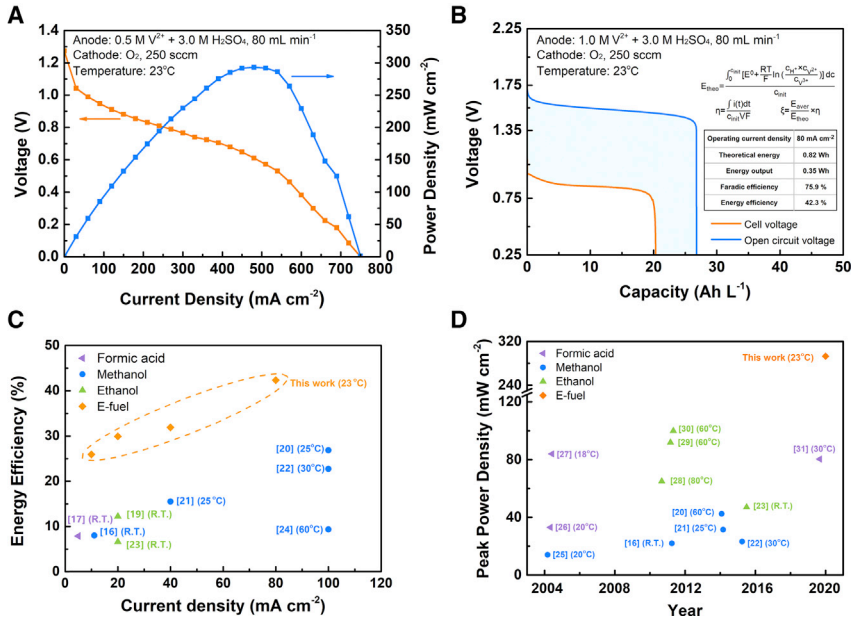

Figure 3. The E-fuel Cell Performance at Room Temperature

(A) Polarization and power density curves with a peak current density of 750 mA cm^{-2} and a peak power density of 293 mW cm^{-2}.

(B) Constant-current discharging behavior with an energy efficiency of 42.3%.

(C and D) Energy efficiency (C) and peak power density (D) comparisons of various direct liquid fuel cells.

See also Tables S1 and S2 for detailed performance comparisons.

formation of oxygen functional groups further improves the hydrophilicity and thus increases the effective surface area.[53,57,58] Thus, this striking feature ensures that the e-fuel cell will have cost-effectiveness and durability.[53] It should also be mentioned that radically different from the catalyst layer made of granular materials in conventional DLFCs, the anode catalyst layer of this direct liquid e-fuel cell is made of fibrous graphite-felt materials, which has a dual-scaled pore structure (primary pores formed by voids among the fibers and secondary pores inside fibers created by thermal treatment).[59,60]

General Performance

As shown in Figures 3A and 3B, it has been experimentally demonstrated that the present direct liquid e-fuel cell, consisting of a catalyst-free graphite-felt anode and a conventional oxygen cathode separated by a proton exchange membrane, results in an OCV of 1.23 V, a maximum current density of 750 mA cm^{-2}, a peak power density of 293 mW cm^{-2}, and an energy efficiency of 42.3% at room temperature. The e-fuel cell performance is much higher than those of the conventional DLFCs previously reported in the open literature, as shown in Figures 3C and 3D.[16–31] It is worth mentioning that the OCV (1.23 V) of this direct liquid e-fuel cell is lower than the theoretical voltage (1.49 V), which mainly results from the activation loss and the fuel crossover. In this e-fuel cell, the cathodic reaction (oxygen reduction[61]) predominates over the activation loss due to the super-fast anodic reaction (vanadium ion oxidation[38]). Meanwhile, the membrane is permeable to vanadium ions in addition to protons, and thus the presence of vanadium ions at the cathode leads to a mixed potential created by simultaneous vanadium-ion oxidation and oxygen reduction.[62] As such, the loss of 0.26 V under an open-circuit condition is mainly

caused by the cathode. Compared to conventional liquid fuels such as methanol and ethanol, the present e-fuel is electrically rechargeable, which allows operation for >100 cycles, greatly reducing the fuel production cost to as low as US$0.01 L^{-1} per refueling, as shown in Table S3, proving it to be a cost-effective alternative fuel. Furthermore, for some liquid fuels such as ethanol, due to the existence of the strong C–C bond, the fuel cell could present only a low energy efficiency (normally lower than 30%, as shown in Table S1). What is worse is that the conventional DLFCs always require noble metal catalysts in preparing the anode but show a very limited power density (normally a few tens of milliwatts per square centimeter, as shown in Table S2), primarily because of the sluggish electrochemical kinetics of liquid fuel oxidation reaction on the existing electrocatalysts. The present e-fuel is highly reactive even on carbon-based materials. This not only dramatically boosts the e-fuel cell performance and thus makes the system both powerful and efficient but it also eliminates the use of any noble metal catalysts, thus making the power-generation system both cost-effective and durable, with a system cost estimation per unit power as low as US$640.67 kW^{-1} (as shown in Table S4). Hence, the direct liquid e-fuel cell with its fast recharging is a powerful, efficient, cost-effective, and durable power-generation device. This emerging technology has great potential for widespread commercialization in the future FCEV industry.

Effect of the E-fuel Solution Composition on the E-fuel Cell Performance

Figures 4A and 4B show the performance of the direct liquid e-fuel cell fed with the e-fuel solution containing various concentrations of V^{2+} ions, ranging from 0.1 to 1.0 M. It is noted that the e-fuel cell performance is improved by increasing the V^{2+} ion concentration from 0.1 to 0.5 M, while a further increase to 1.0 M decreases the e-fuel cell performance, yielding its best performance at 0.5 M V^{2+} ions in the e-fuel solution—a peak power density of 278 mW cm^{-2} and a maximum current density of 690 mA cm^{-2}, respectively, at room temperature. Such superior performance is mainly attributed to the fast reaction kinetics of the highly reactive e-fuel solution, even on carbon-based materials. Increasing the V^{2+} ion concentration from 0.1 to 0.5 M not only enhances the mass transport of V^{2+} ions from the anode flow field to the electrode surface, lowering the concentration loss, but also accelerates the interfacial reaction kinetics, seen by the electrochemical impedance spectroscopy (EIS) results in Figure 4C and Table S5, reducing the activation loss and thus boosting the e-fuel cell performance.[63] However, a further increase to 1.0 M slightly degrades the e-fuel cell performance because of an increase in the charge transfer resistance, as shown in Figure 4C and Table S5. Hence, a 0.5-M operation results in the fastest anodic kinetics, which is consistent with many previous experimental investigations.[64,65]

Effect of the E-fuel Solution Flow Rate on the E-fuel Cell Performance

The flow rate of the e-fuel solution is another important operating parameter that affects the mass transport process and thus the e-fuel cell performance.[66] The experiments were conducted at flow rates ranging from 5 to 80 mL min^{-1}, fed with the e-fuel solution containing 0.5 and 1.0 M V^{2+} ions, respectively. It is seen in Figures 4D and 4E that, when the e-fuel cell was fed with the e-fuel containing 1.0 M V^{2+} ions, the peak power density was increased from 247 to 281 mW cm^{-2} as the flow rate was increased from 5 to 80 mL min^{-1}; this is attributed to the enhanced mass transport of reactants and the reduced charge transfer resistance, as evidenced by the EIS results in Table S6. It is also worth noting from Figures 4D and 4E that when the flow rate exceeds 60 mL min^{-1}, no obvious performance improvement can be observed, confirming the notion that a sufficient reactant concentration on the porous electrode surface is achieved. Hence, it is believed that the flow rate of 60 mL min^{-1}

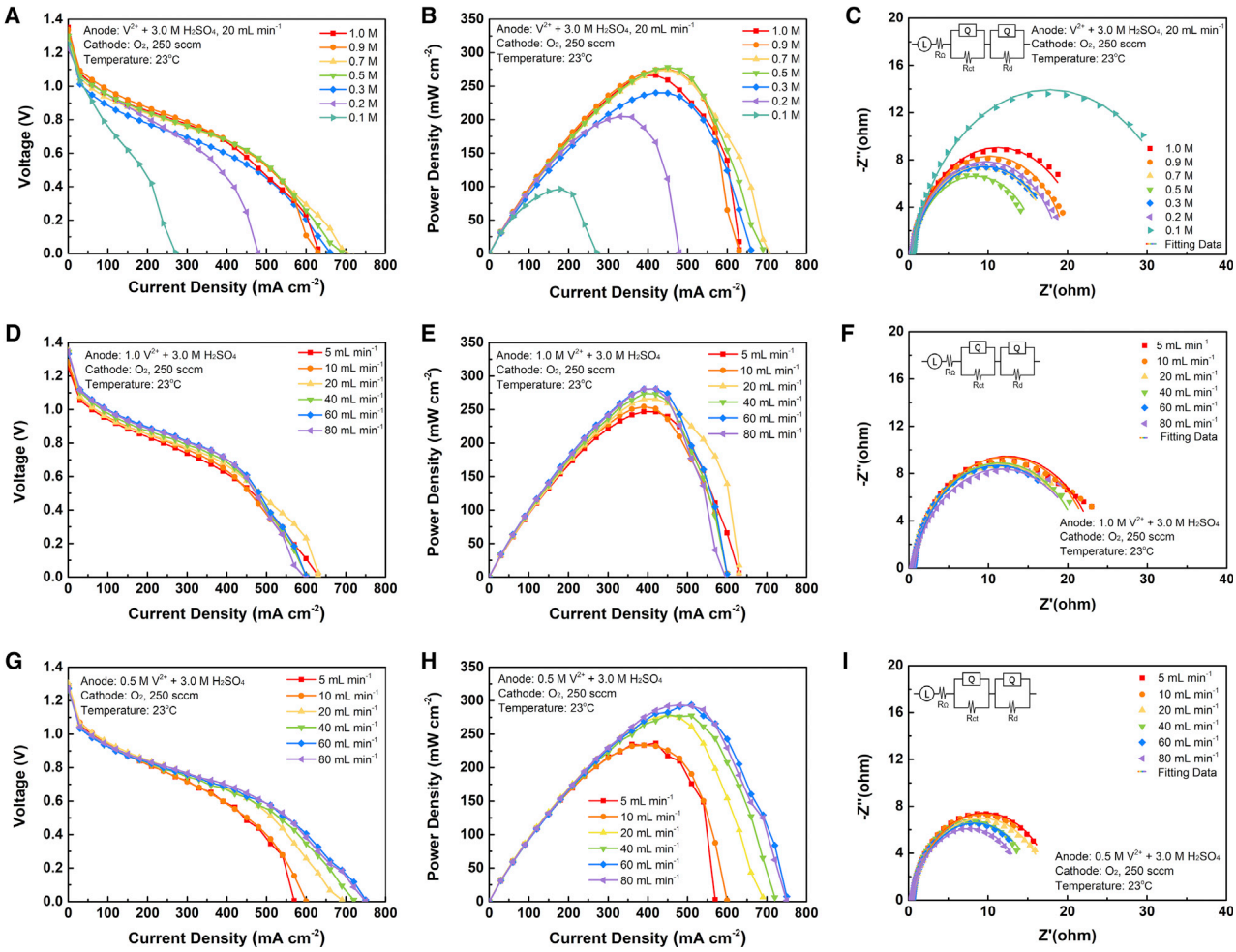

Figure 4. Effects of the Operating Parameters on the E-fuel Cell Performance

(A–C) The effect of the e-fuel composition on the (A) voltage, (B) power density, and (C) charge transfer resistance. The optimal e-fuel composition contains 0.5 M V^{2+} ions.

(D–F) The effect of the e-fuel (containing 1.0 M V^{2+} ions) flow rate on the (D) voltage, (E) power density, and (F) charge transfer resistance. The optimal flow rate is 60 mL min^{-1}.

(G–I) The effect of the e-fuel (containing 0.5 M V^{2+} ions) flow rate on the (G) voltage, (H) power density, and (I) charge transfer resistance. The optimal flow rate is 60 mL min^{-1}.

See also Tables S5 and S6 for detailed charge transfer resistances.

can be the best choice for this e-fuel cell to achieve its best performance while maintaining a higher system efficiency with a relatively lower pump power consumption.[67,68] Similarly, when the present e-fuel cell was fed with 0.5 M V^{2+} ions, the performance was also upgraded with the e-fuel solution flow rate—the maximum current density from 570 to 750 mA cm^{-2} and the peak power density from 237 to 293 mW cm^{-2}, as shown in Figures 4G and 4H. Further attention paid to the EIS results in Figure 4I and Table S6 confirms that while the e-fuel solution flow rate has an insignificant effect on the ohmic resistance of the e-fuel cell, it can reduce the mass transport resistance, consequently being an important factor that greatly influences the charge transfer resistance and in turn the e-fuel cell performance.

Constant-Current Discharging Behavior

The constant-current discharging behavior of the present direct liquid e-fuel cell is examined at 4 different operating current densities: 10, 20, 40, and 80 mA cm^{-2},

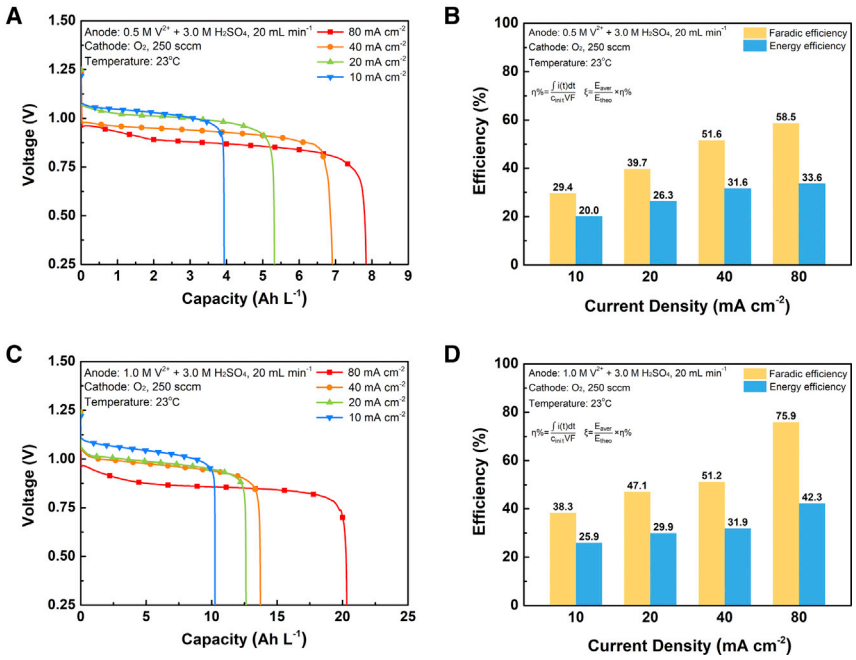

Figure 5. Constant-Current Discharging Behaviors of This E-fuel Cell

(A and B) Discharge voltage (A) and Faradic efficiency and energy efficiency (B) for using the e-fuel containing 0.5 M V^{2+} ions at the current density range from 10 to 80 mA cm^{-2}.

(C and D) Discharge voltage (C) and Faradic efficiency and energy efficiency (D) for using the e-fuel containing 1.0 M V^{2+} ions at the current density range from 10 to 80 mA cm^{-2}.

The peak energy efficiency of 42.3% is achieved at a current density of 80 mA cm^{-2}.

See also Figures S1–S8 for detailed calculations of Faradic efficiency and energy efficiency.

fed with the e-fuel solution containing 0.5 and 1.0 M V^{2+} ions, respectively, as shown in Figures 5A and 5C. It is observed that a higher constant-current operation slightly lowers the voltage plateau but largely increases the energy output (achieved energy capacity). On the one hand, a higher constant-current operation results in a shorter duration for the e-fuel cell discharging and thus alleviates the negative self-discharging, resulting in a larger discharging energy capacity. On the other hand, increasing the constant-current density leads to a larger ohmic loss, thereby lowering the voltage plateau. In this e-fuel cell, the membrane is also permeable to vanadium ions in addition to protons, but the presence of the e-fuel solution on the Pt surface of the cathode leads to the mixed potential[62] created by the simultaneous vanadium ion oxidation and oxygen reduction and the self-discharging, referring to the loss of energy stored in the e-fuel solution.[14,69] Hence, to alleviate the e-fuel crossover phenomenon, a thick Nafion 117 membrane has been used in this direct liquid e-fuel cell fabrication. In addition, previous investigations have shown that the vanadium ion permeability of the Nafion 117 membrane is 35.6 × 10^{-7} cm^2 min^{-1}, with a proton conductivity of 58.7 mS cm^{-1}.[70] Alternatively, another effective approach to alleviate the e-fuel crossover is to develop membranes with a higher ion selectivity. It is also worth mentioning that the proton concentration in the e-fuel solution determines the ionic conductivities of both the e-fuel solution and the proton exchange membrane,[71] which thus further influences the e-fuel cell performance. It can be estimated that, based on the anodic reaction, even if 1.0 M V^{2+} ions in the e-fuel solution are completely consumed, the proton concentration will only decrease from 6.0 to 5.0 M.

Energy Efficiency of the Present E-fuel Cell

As shown in Figure 5D, for the e-fuel cell running with 1.0 M V^{2+} ions, the Faradic efficiency was increased from 38.3% to 75.9% by increasing the constant-current density from 10 to 80 mA cm^{-2} due to the shorter discharging duration at a higher constant-current density. The energy losses and energy efficiencies at various constant-current densities are summarized in Figures S1–S4 (with 1.0 M V^{2+} ions) and Figures S5–S8 (with 0.5 M V^{2+} ions), respectively. For example, the e-fuel cell running on the e-fuel solution containing 1.0 M V^{2+} ions, the energy efficiencies of 25.9%, 29.9%, 31.9%, and 42.3% were achieved at constant-current densities of 10, 20, 40, and 80 mA cm^{-2}, respectively, as shown in Figure 5D. In some conventional liquid fuels such as ethanol, the existence of the strong C–C bond leads to a limited energy efficiency (<30%, as shown in Table S1) and a low peak power density (<100 mW cm^{-2}, as shown in Table S2), even at temperatures up to 80°C, seriously limiting the widespread application of conventional DLFCs. Hence, the present e-fuel cell exhibits an energy efficiency of 42.3% at a current density of 80 mA cm^{-2}, even at room temperature (i.e., 23°C), indicating that the present e-fuel cell is a promising candidate for powering future FCEVs. It should be mentioned that the energy density of the e-fuel solution (as shown in Table S3) is still lower than other liquid organic fuels, which is seriously limited by the vanadium ion solubility (e.g., 3.28 M at 20°C[72]) and 1 electron release per vanadium ion. Hence, it will be critical to screen and develop the e-fuel solution with a higher energy density in the future.

In this work, we have demonstrated a power-generation system: the direct liquid e-fuel cell, which is capable of efficiently converting e-fuel to electricity at a high rate. Experimentally, it is shown that the present direct liquid e-fuel cell, consisting of a catalyst-free graphite-felt anode and a conventional oxygen cathode separated by a proton exchange membrane, results in an open-circuit voltage of 1.23 V, a maximum current density of 750 mA cm^{-2}, a peak power density of 293 mW cm^{-2}, and an energy efficiency of 42.3% at room temperature, all of which are much higher than the previously reported performances of conventional DLFCs. Such an improvement opens a window for breakthroughs in the development of this emerging e-fuel cell technology.

In summary, this direct liquid e-fuel cell with its fast recharging is a powerful, efficient, cost-effective, and durable power-generation device. This emerging technology is closer to reality, particularly in the fuel cell electric vehicle industry.

EXPERIMENTAL PROCEDURES

Resource Availability

Lead Contact

Further information and requests for data and resources should be directed to and be fulfilled by the Lead Contact, Liang An (liang.an@polyu.edu.hk).

Materials Availability

This study did not generate new unique reagents.

Data and Code Availability

This study did not generate/analyze datasets and code.

Preparation of Membrane Electrode Assembly

An MEA consisting of two homemade electrodes is separated by a commercial proton exchange membrane in this work. A homemade Pt/C-coated carbon paper was used as the conventional oxygen cathode, which was prepared using a method

reported elsewhere.[73] The commercial catalysts, 60 wt% Pt/C (Johnson Matthey), were mixed with 5.0 wt% Nafion (Fuel Cell Store) as the binder and ethanol as the solvent to form the catalyst ink, which was dispersed in an ultrasonic bath for 30 min. Then, the as-prepared ink was sprayed onto a piece of carbon paper that serves as the backing layer. The metallic loading on the cathode was ~0.5 mg cm^{-2}. A graphite felt (AvCarb G100, Fuel Cell Store) was heated at 500°C for 5 h to improve its wettability and activity[53,74] as the catalyst-free graphite-felt anode. The geometric area for both the anode and the cathode was 2.0 × 2.0 cm. The Nafion 117 membrane as the proton exchange membrane was cut into a 3.0 × 3.0 cm piece and treated using standard procedures.[75] The membrane was boiled for 1 h in 3.0 wt% H_2O_2 solution and then for 1 h in deionized (DI) water. Afterward, it was boiled for 1 h in 1.0 M H_2SO_4 and again for 1 h in the DI water. Finally, it was stored in the DI water before further use.

E-fuel Cell Setup and Instrumentation

To evaluate the e-fuel cell performance, an e-fuel cell fixture was fabricated, as shown in Figures 1B and 1C. Each side of this e-fuel cell fixture includes a plastic-made endplate, an aluminum heating plate, an Au-coated Cu current collector, and a graphite flow field. Several polytetrafluoroethylene (PTFE) gaskets were placed among components to avoid the gas and liquid leakage. The serpentine flow field with an area of 2.0 × 2.0 cm was engraved on the graphite to provide the e-fuel-oxygen flowing channel. An oxygen cylinder was connected to the cathode flow channel to supply the oxygen, and a mass flowmeter (Cole-Parmer) was installed to control the oxygen flow rate at 250 sccm. To prepare the e-fuel solution containing V^{2+} ions, vanadyl sulfate powder was dissolved in sulfuric acid to form a mixed solution,[76] and then an electrochemical flow cell setup was used to convert VO^{2+} ions to V^{2+} ions[77,78] using a 20-mL e-fuel solution with a flow rate of 52 mL min^{-1}.

The polarization curves and constant-current discharging curves of the e-fuel cell were recorded using an electric load (Arbin BT2000, Arbin Instruments). It should be mentioned that the e-fuel solution was kept circulating between the e-fuel cell and the e-fuel tank. The fuel utilization efficiency, Faradic efficiency η is calculated with Equation 4:[79]

$$\eta = \frac{\int i(t)dt}{c_{init}VF}, \qquad \text{(Equation 4)}$$

where t is the duration of the discharging process, $i(t)$ is the discharging current; c_{init} represents the initial concentration of V^{2+} ions in the e-fuel solution, V is the volume of the e-fuel solution, and F is the Faraday constant. The energy efficiency ξ is calculated based on the product of the voltage efficiency ($\varphi = \frac{E_{aver}}{E_{theo}}$) and Faradic efficiency (η):[79]

$$\xi = \varphi \times \eta = \frac{E_{aver}}{E_{theo}} \times \eta, \qquad \text{(Equation 5)}$$

where E_{aver} is the average discharging voltage, while E_{theo} is the theoretical average voltage. ΔE is the theoretical voltage that is calculated based on the Nernst equation as[80]

$$\Delta E = E_c^0 - \frac{RT}{nF} ln\left(\frac{\prod a_{products}^{v_i}}{\prod a_{reactants}^{v_i}}\right) - E_a^0 - \frac{RT}{nF} ln\left(\frac{\prod b_{products}^{v_i}}{\prod b_{reactants}^{v_i}}\right) = E^0 + \frac{RT}{F} ln\left(\frac{c_{H^+} \times c_{V^{2+}}}{c_{V^{3+}}}\right) \qquad \text{(Equation 6)}$$

and

$$E_{theo} = \frac{\int_0^{c_{init}} \Delta E dc}{c_{init}} = \frac{\int_0^{c_{init}} \left[E^0 + \frac{RT}{F} \ln\left(\frac{c_{H^+} \times c_{V^{2+}}}{c_{V^{3+}}}\right)\right] dc}{c_{init}}, \quad \text{(Equation 7)}$$

where R is the universal gas constant and T is the absolute temperature.

An electrochemical workstation (CHI-605C, CH Instruments) was used to conduct the EIS and CV tests. The EIS tests were conducted with a frequency range between 0.01 and 10^5 Hz. The CV tests were conducted by a three-electrode electrochemical cell, in which the graphite felt (both of pristine graphite felt and thermally treated graphite felt), Pt mesh, and saturated calomel electrode (SCE) were used as the working electrode, the counter electrode, and the reference electrode, respectively. The e-fuel solution for CV tests is an aqueous solution containing 0.1 M V^{2+} ions and 1.5 M H_2SO_4, and the voltage range was 0.1 to −1.0 V.

SUPPLEMENTAL INFORMATION

Supplemental Information can be found online at https://doi.org/10.1016/j.xcrp.2020.100102.

ACKNOWLEDGMENTS

The work described in this paper was fully supported by a grant from the Research Grant Council of the Hong Kong Special Administrative Region, China (Project No. T23-601/17-R).

AUTHOR CONTRIBUTIONS

Conceptualization, L.A.; Methodology, L.A. and X.S.; Investigation, X.S., X.H., Y.M., and Z.P.; Writing – Original Draft, X.S., Z.P., and L.A.; Writing – Review & Editing, X.S., X.H., Z.P., and L.A.; Supervision, L.A.

DECLARATION OF INTERESTS

The authors declare no competing interests.

Received: March 2, 2020
Revised: April 23, 2020
Accepted: May 21, 2020
Published: July 1, 2020

REFERENCES

1. Lee, Y.M. (2016). Fuel cells: operating flexibly. Nat. Energy *1*, 1–2.
2. Cano, Z.P., Banham, D., Ye, S., Hintennach, A., Lu, J., Fowler, M., and Chen, Z. (2018). Batteries and fuel cells for emerging electric vehicle markets. Nat. Energy *3*, 279–289.
3. Wang, S., and Jiang, S.P. (2017). Prospects of fuel cell technologies. Natl. Sci. Rev. *4*, 163–166.
4. Chen, Y., Ji, S., Zhao, S., Chen, W., Dong, J., Cheong, W.C., Shen, R., Wen, X., Zheng, L., Rykov, A.I., et al. (2018). Enhanced oxygen reduction with single-atomic-site iron catalysts for a zinc-air battery and hydrogen-air fuel cell. Nat. Commun. *9*, 5422.
5. Chen, Z. (2020). Water balancing. Nat. Energy *5*, 12–13.
6. Proietti, E., Jaouen, F., Lefèvre, M., Larouche, N., Tian, J., Herranz, J., and Dodelet, J.P. (2011). Iron-based cathode catalyst with enhanced power density in polymer electrolyte membrane fuel cells. Nat. Commun. *2*, 416.
7. Staffell, I., Scamman, D., Abad, A.V., Balcombe, P., Dodds, P.E., Ekins, P., Shah, N., and Ward, K.R. (2019). The role of hydrogen and fuel cells in the global energy system. Energy Environ. Sci. *12*, 463–491.
8. Setzler, B.P., Zhuang, Z., Wittkopf, J.A., and Yan, Y. (2016). Activity targets for nanostructured platinum-group-metal-free catalysts in hydroxide exchange membrane fuel cells. Nat. Nanotechnol. *11*, 1020–1025.
9. An, L., Zhao, T., Li, Y., and Wu, Q. (2012). Charge carriers in alkaline direct oxidation fuel cells. Energy Environ. Sci. *5*, 7536–7538.
10. An, L., Zhao, T., and Li, Y. (2015). Carbon-neutral sustainable energy technology: direct ethanol fuel cells. Renew. Sustain. Energy Rev. *50*, 1462–1468.
11. Scofield, M.E., Liu, H., and Wong, S.S. (2015). A concise guide to sustainable PEMFCs: recent advances in improving both oxygen reduction catalysts and proton exchange membranes. Chem. Soc. Rev. *44*, 5836–5860.
12. Wang, Z., Parrondo, J., He, C., Sankarasubramanian, S., and Ramani, V. (2019). Efficient pH-gradient-enabled microscale bipolar interfaces in direct borohydride fuel cells. Nat. Energy *4*, 281–289.
13. Yu, E.H., Wang, X., Krewer, U., Li, L., and Scott, K. (2012). Direct oxidation alkaline fuel cells: from materials to systems. Energy Environ. Sci. *5*, 5668–5680.

14. Lu, S., Wu, C., Liang, D., Tan, Q., and Xiang, Y. (2014). Layer-by-layer self-assembly of Nafion–[CS–PWA] composite membranes with suppressed vanadium ion crossover for vanadium redox flow battery applications. RSC Advances *4*, 24831–24837.

15. Cheng, Y., Zhang, J., Lu, S., and Jiang, S.P. (2020). Significantly enhanced performance of direct methanol fuel cells at elevated temperatures. J. Power Sources *450*, 227620.

16. Feng, L., Zhang, J., Cai, W., Xing, W., and Liu, C. (2011). Single passive direct methanol fuel cell supplied with pure methanol. J. Power Sources *196*, 2750–2753.

17. Hong, P., Luo, F., Liao, S., and Zeng, J. (2011). Effects of Pt/C, Pd/C and PdPt/C anode catalysts on the performance and stability of air breathing direct formic acid fuel cells. Int. J. Hydrogen Energy *36*, 8518–8524.

18. Hong, P., Liao, S., Zeng, J., and Huang, X. (2010). Design, fabrication and performance evaluation of a miniature air breathing direct formic acid fuel cell based on printed circuit board technology. J. Power Sources *195*, 7332–7337.

19. Bambagioni, V., Bianchini, C., Chen, Y., Filippi, J., Fornasiero, P., Innocenti, M., Lavacchi, A., Marchionni, A., Oberhauser, W., and Vizza, F. (2012). Energy efficiency enhancement of ethanol electrooxidation on Pd-CeO(2)/C in passive and active polymer electrolyte-membrane fuel cells. ChemSusChem *5*, 1266–1273.

20. Li, Y., Zhang, X., Nie, L., Zhang, Y., and Liu, X. (2014). Stainless steel fiber felt as cathode diffusion backing and current collector for a micro direct methanol fuel cell with low methanol crossover. J. Power Sources *245*, 520–528.

21. Cao, J., Wang, L., Song, L., Xu, J., Wang, H., Chen, Z., Huang, Q., and Yang, H. (2014). Novel cathodal diffusion layer with mesoporous carbon for the passive direct methanol fuel cell. Electrochim. Acta *118*, 163–168.

22. Deng, H., Zhang, Y., Zheng, X., Li, Y., Zhang, X., and Liu, X. (2015). A CNT (carbon nanotube) paper as cathode gas diffusion electrode for water management of passive μ-DMFC (micro-direct methanol fuel cell) with highly concentrated methanol. Energy *82*, 236–241.

23. Wang, L., Lavacchi, A., Bevilacqua, M., Bellini, M., Fornasiero, P., Filippi, J., Innocenti, M., Marchionni, A., Miller, H.A., and Vizza, F. (2015). Energy efficiency of alkaline direct ethanol fuel cells employing nanostructured palladium electrocatalysts. ChemCatChem *7*, 2214–2221.

24. Yuan, Z., Chuai, W., Guo, Z., Tu, Z., and Kong, F. (2019). Investigation of self-adaptive thermal control design in passive direct methanol fuel cell. Energy Stor. *1*, e64.

25. Jiang, R., Rong, C., and Chu, D. (2004). Determination of energy efficiency for a direct methanol fuel cell stack by a fuel circulation method. J. Power Sources *126*, 119–124.

26. Ha, S., Adams, B., and Masel, R. (2004). A miniature air breathing direct formic acid fuel cell. J. Power Sources *128*, 119–124.

27. Zhu, Y., Ha, S.Y., and Masel, R.I. (2004). High power density direct formic acid fuel cells. J. Power Sources *130*, 8–14.

28. Tadanaga, K., Furukawa, Y., Hayashi, A., and Tatsumisago, M. (2010). Direct ethanol fuel cell using hydrotalcite clay as a hydroxide ion conductive electrolyte. Adv. Mater. *22*, 4401–4404.

29. Shen, S., Zhao, T., Xu, J., and Li, Y. (2011). High performance of a carbon supported ternary PdIrNi catalyst for ethanol electro-oxidation in anion-exchange membrane direct ethanol fuel cells. Energy Environ. Sci. *4*, 1428–1433.

30. An, L., and Zhao, T. (2011). An alkaline direct ethanol fuel cell with a cation exchange membrane. Energy Environ. Sci. *4*, 2213–2217.

31. Abd Lah Halim, F., Tsujiguchi, T., Osaka, Y., and Kodama, A. (2019). Performance of direct formic acid fuel cell using transition metal-nitrogen-doped carbon nanotubes as cathode catalysts. Int. J. Energy Res. *43*, 8070–8084.

32. Demirci, U.B. (2007). Direct liquid-feed fuel cells: thermodynamic and environmental concerns. J. Power Sources *169*, 239–246.

33. Chang, J., Feng, L., Liu, C., Xing, W., and Hu, X. (2014). Ni_2P enhances the activity and durability of the Pt anode catalyst in direct methanol fuel cells. Energy Environ. Sci. *7*, 1628–1632.

34. Zhao, X., Yin, M., Ma, L., Liang, L., Liu, C., Liao, J., Lu, T., and Xing, W. (2011). Recent advances in catalysts for direct methanol fuel cells. Energy Environ. Sci. *4*, 2736–2753.

35. Ho, V.T., Pillai, K.C., Chou, H., Pan, C., Rick, J., Su, W., Hwang, B., Lee, J., Sheu, H., and Chuang, W. (2011). Robust non-carbon $Ti_{0.7}Ru_{0.3}O_2$ support with co-catalytic functionality for Pt: enhances catalytic activity and durability for fuel cells. Energy Environ. Sci. *4*, 4194–4200.

36. Li, W., Yu, A., Higgins, D.C., Llanos, B.G., and Chen, Z. (2010). Biologically inspired highly durable iron phthalocyanine catalysts for oxygen reduction reaction in polymer electrolyte membrane fuel cells. J. Am. Chem. Soc. *132*, 17056–17058.

37. Xu, C., Wang, H., Shen, P.K., and Jiang, S.P. (2007). Highly ordered Pd nanowire arrays as effective electrocatalysts for ethanol oxidation in direct alcohol fuel cells. Adv. Mater. *19*, 4256–4259.

38. Jiang, H., Wei, L., Fan, X., Xu, J., Shyy, W., and Zhao, T. (2019). A novel energy storage system incorporating electrically rechargeable liquid fuels as the storage medium. Sci. Bull. (Beijing) *64*, 270–280.

39. Amine, K. (2019). E-fuel system: a conceptual breakthrough for energy storage. Sci. Bull. (Beijing) *64*, 227–228.

40. Younesi, R., Veith, G.M., Johansson, P., Edström, K., and Vegge, T. (2015). Lithium salts for advanced lithium batteries: Li–metal, Li–O_2, and Li–S. Energy Environ. Sci. *8*, 1905–1922.

41. Fan, X., Ji, X., Chen, L., Chen, J., Deng, T., Han, F., Yue, J., Piao, N., Wang, R., and Zhou, X. (2019). All-temperature batteries enabled by fluorinated electrolytes with non-polar solvents. Nat. Energy *4*, 882–890.

42. Shi, X., Sun, Q., Boateng, B., Niu, Y., Han, Y., Lv, W., and He, W. (2019). A quasi-solid composite separator with high ductility for safe and high-performance lithium-ion batteries. J. Power Sources *414*, 225–232.

43. Bai, P., Li, J., Brushett, F.R., and Bazant, M.Z. (2016). Transition of lithium growth mechanisms in liquid electrolytes. Energy Environ. Sci. *9*, 3221–3229.

44. Liu, J., Shi, X., Boateng, B., Han, Y., Chen, D., and He, W. (2019). A Highly Stable Separator from an Instantly Reformed Gel with Direct Post-Solidation for Long-Cycle High-Rate Lithium-Ion Batteries. ChemSusChem *12*, 908–914.

45. Zhao, Y., Setzler, B.P., Wang, J., Nash, J., Wang, T., Xu, B., and Yan, Y. (2019). An efficient direct ammonia fuel cell for affordable carbon-neutral transportation. Joule *3*, 2472–2484.

46. Grosse Austing, J., Kirchner, C.N., Hammer, E.M., Komsiyska, L., and Wittstock, G. (2015). Study of an unitised bidirectional vanadium/air redox flow battery comprising a two-layered cathode. J. Power Sources *273*, 1163–1170.

47. An, L., Chai, Z., Zeng, L., Tan, P., and Zhao, T. (2013). Mathematical modeling of alkaline direct ethanol fuel cells. Int. J. Hydrogen Energy *38*, 14067–14075.

48. Park, M., Ryu, J., Wang, W., and Cho, J. (2017). Material design and engineering of next-generation flow-battery technologies. Nat. Rev. Mater. *2*, 16080.

49. Shukla, A., Jackson, C., Scott, K., and Raman, R. (2002). An improved-performance liquid-feed solid-polymer-electrolyte direct methanol fuel cell operating at near-ambient conditions. Electrochim. Acta *47*, 3401–3407.

50. Shukla, A., Raman, R., Choudhury, N., Priolkar, K., Sarode, P., Emura, S., and Kumashiro, R. (2004). Carbon-supported Pt–Fe alloy as a methanol-resistant oxygen-reduction catalyst for direct methanol fuel cells. J. Electroanal. Chem. (Lausanne Switz.) *563*, 181–190.

51. An, L., and Chen, R. (2016). Recent progress in alkaline direct ethylene glycol fuel cells for sustainable energy production. J. Power Sources *329*, 484–501.

52. Jiang, H., Sun, J., Wei, L., Wu, M., Shyy, W., and Zhao, T. (2020). A high power density and long cycle life vanadium redox flow battery. Energy Stor. Mater. *24*, 529–540.

53. Sun, B., and Skyllas-Kazacos, M. (1992). Modification of graphite electrode materials for vanadium redox flow battery application—I. Thermal treatment. Electrochim. Acta *37*, 1253–1260.

54. Zeng, L., Zhao, T., and Wei, L. (2018). Revealing the performance enhancement of oxygenated carbonaceous materials for vanadium redox flow batteries: functional groups or specific surface area? Adv. Sustain. Syst. *2*, 1700148.

55. Mazúr, P., Mrlík, J., Beneš, J., Pocedič, J., Vrána, J., Dundálek, J., and Kosek, J. (2018). Performance evaluation of thermally treated graphite felt electrodes for vanadium redox flow battery and their four-point single cell characterization. J. Power Sources *380*, 105–114.

56. Kil, D., Lee, H.J., Park, S., Kim, S., and Kim, H. (2017). Synthesis of activated graphite felts using short-term ozone/heat treatment for vanadium redox flow batteries. J. Electrochem. Soc. *164*, A3011.

57. Kim, K.J., Kim, Y.-J., Kim, J.-H., and Park, M.-S. (2011). The effects of surface modification on carbon felt electrodes for use in vanadium redox flow batteries. Mater. Chem. Phys. *131*, 547–553.

58. Kim, K.J., Park, M.-S., Kim, Y.-J., Kim, J.H., Dou, S.X., and Skyllas-Kazacos, M. (2015). A technology review of electrodes and reaction mechanisms in vanadium redox flow batteries. J. Mater. Chem. A Mater. Energy Sustain. *3*, 16913–16933.

59. Jiang, H., Shyy, W., Wu, M., Zhang, R., and Zhao, T. (2019). A bi-porous graphite felt electrode with enhanced surface area and catalytic activity for vanadium redox flow batteries. Appl. Energy *233*, 105–113.

60. Castañeda, L.F., Walsh, F.C., Nava, J.L., and de Leon, C.P. (2017). Graphite felt as a versatile electrode material: properties, reaction environment, performance and applications. Electrochim. Acta *258*, 1115–1139.

61. Silva, V.B., and Rouboa, A. (2012). Hydrogen-fed PEMFC: overvoltage analysis during an activation procedure. J. Electroanal. Chem. (Lausanne Switz.) *671*, 58–66.

62. Paganin, V.A., Sitta, E., Iwasita, T., and Vielstich, W. (2005). Methanol crossover effect on the cathode potential of a direct PEM fuel cell. J. Appl. Electrochem. *35*, 1239–1243.

63. Aaron, D., Tang, Z., Papandrew, A.B., and Zawodzinski, T.A. (2011). Polarization curve analysis of all-vanadium redox flow batteries. J. Appl. Electrochem. *41*, 1175.

64. Xu, Q., Zhao, T., and Zhang, C. (2014). Effects of SOC-dependent electrolyte viscosity on performance of vanadium redox flow batteries. Appl. Energy *130*, 139–147.

65. You, D., Zhang, H., and Chen, J. (2009). A simple model for the vanadium redox battery. Electrochim. Acta *54*, 6827–6836.

66. Kjeang, E., Proctor, B.T., Brolo, A.G., Harrington, D.A., Djilali, N., and Sinton, D. (2007). High-performance microfluidic vanadium redox fuel cell. Electrochim. Acta *52*, 4942–4946.

67. Tang, A., Bao, J., and Skyllas-Kazacos, M. (2014). Studies on pressure losses and flow rate optimization in vanadium redox flow battery. J. Power Sources *248*, 154–162.

68. Ma, X., Zhang, H., Sun, C., Zou, Y., and Zhang, T. (2012). An optimal strategy of electrolyte flow rate for vanadium redox flow battery. J. Power Sources *203*, 153–158.

69. Garche, J., Dyer, C.K., Moseley, P.T., Ogumi, Z., Rand, D.A., and Scrosati, B. (2013). Encyclopedia of Electrochemical Power Sources (Newnes).

70. Xi, J., Wu, Z., Teng, X., Zhao, Y., Chen, L., and Qiu, X. (2008). Self-assembled polyelectrolyte multilayer modified Nafion membrane with suppressed vanadium ion crossover for vanadium redox flow batteries. J. Mater. Chem. *18*, 1232–1238.

71. Yang, W., He, Y., and Li, Y. (2015). Performance modeling of a vanadium redox flow battery during discharging. Electrochim. Acta *155*, 279–287.

72. Rahman, F., and Skyllas-Kazacos, M. (1998). Solubility of vanadyl sulfate in concentrated sulfuric acid solutions. J. Power Sources *72*, 105–110.

73. An, L., and Zhao, T.S. (2011). Performance of an alkaline-acid direct ethanol fuel cell. Int. J. Hydrogen Energy *36*, 9994–9999.

74. Jiang, H., Shyy, W., Zeng, L., Zhang, R., and Zhao, T. (2018). Highly efficient and ultra-stable boron-doped graphite felt electrodes for vanadium redox flow batteries. J. Mater. Chem. A Mater. Energy Sustain. *6*, 13244–13253.

75. Jiang, B., Wu, L., Yu, L., Qiu, X., and Xi, J. (2016). A comparative study of Nafion series membranes for vanadium redox flow batteries. J. Membr. Sci. *510*, 18–26.

76. Zeng, L., Zhao, T., Wei, L., Zeng, Y., and Zhang, Z. (2016). Highly stable pyridinium-functionalized cross-linked anion exchange membranes for all vanadium redox flow batteries. J. Power Sources *331*, 452–461.

77. Jiang, H.R., Shyy, W., Wu, M.C., Wei, L., and Zhao, T.S. (2017). Highly active, bi-functional and metal-free B_4C-nanoparticle-modified graphite felt electrodes for vanadium redox flow batteries. J. Power Sources *365*, 34–42.

78. Xu, Q., and Zhao, T.S. (2013). Determination of the mass-transport properties of vanadium ions through the porous electrodes of vanadium redox flow batteries. Phys. Chem. Chem. Phys. *15*, 10841–10848.

79. Liu, J., Zhao, T.-S., Chen, R., and Wong, C.W. (2005). Effect of methanol concentration on passive DMFC performance. Fuel Cells Bull. *2005*, 12–17.

80. Knehr, K., and Kumbur, E. (2011). Open circuit voltage of vanadium redox flow batteries: Discrepancy between models and experiments. Electrochem. Commun. *13*, 342–345.